Chemico-Biological Interactions 310 (2019) 108715

Contents lists available at ScienceDirect

Chemico-Biological Interactions

journal homepage: www.elsevier.com/locate/chembioint

Molecular dynamics simulations of the interaction of Mouse and *Torpedo* acetylcholinesterase with covalent inhibitors explain their differential reactivity: Implications for drug design

Nellore Bhanu Chandar[a], Irena Efremenko[a], Israel Silman[b,**], Jan M.L. Martin[a], Joel L. Sussman[c,*]

[a] Dept. of Organic Chemistry, Weizmann Institute of Science, 7610001, Reḥovot, Israel
[b] Dept. of Neurobiology, Weizmann Institute of Science, 7610001, Reḥovot, Israel
[c] Dept. of Structural Biology and Israel Center for Structural Proteomics, Weizmann Institute of Science, 7610001, Reḥovot, Israel

ARTICLE INFO

Keywords:
Docking
Molecular dynamics
Torpedo californica acetylcholinesterase
Mouse acetylcholinesterase
Phenylmethylsulfonyl fluoride
Benzenesulfonyl fluoride

ABSTRACT

Although the three-dimensional structures of mouse and *Torpedo californica* acetylcholinesterase are very similar, their responses to the covalent sulfonylating agents benzenesulfonyl fluoride and phenylmethylsulfonyl fluoride are qualitatively different. Both agents inhibit the mouse enzyme effectively by covalent modification of its active-site serine. In contrast, whereas the *Torpedo* enzyme is effectively inhibited by benzenesulfonyl fluoride, it is almost completely resistant to phenylmethylsulfonyl fluoride. A bottleneck midway down the active-site gorge in both enzymes restricts access of ligands to the active site at the bottom of the gorge. Molecular dynamics simulations revealed that the mouse enzyme is substantially more flexible than the *Torpedo* enzyme, suggesting that enhanced 'breathing motions' of the mouse enzyme relative to the *Torpedo* enzyme may explain why phenylmethylsulfonyl fluoride can reach the active site in mouse acetylcholinesterase, but not in the *Torpedo* enzyme. Accordingly, we performed docking of the two sulfonylating agents to the two enzymes, followed by molecular dynamics simulations. Whereas benzenesulfonyl fluoride closely approaches the active-site serine in both mouse and *Torpedo* acetylcholinesterase in such simulations, phenylmethylsulfonyl fluoride is able to approach the active-site serine of mouse acetylcholinesterase, but remains trapped above the bottleneck in the *Torpedo* enzyme. Our studies demonstrate that reliance on docking tools in drug design can produce misleading information. Docking studies should, therefore, also be complemented by molecular dynamics simulations in selection of lead compounds. An animated Interactive 3D Complement (I3DC) is available in Proteopedia at http://proteopedia.org/w/Journal:CHEMBIOINT:2.

1. Introduction

The principal biological role of acetylcholinesterase (AChE) is termination of transmission at cholinergic synapses by rapid hydrolysis of the neurotransmitter, acetylcholine (ACh) [1,2].

The crystal structure of *Torpedo californica* acetylcholinesterase (*Tc*AChE) revealed that, despite the high catalytic activity of AChE, which approaches diffusion control [3], its active site is near the bottom of a long and narrow gorge, > 15 Å long, a large part of the surface of which is lined by aromatic residues [4]. Near the mid-point of the gorge is a bottleneck, between two conserved aromatic residues, whose cross-section is smaller than the diameter of the quaternary group of ACh, 6.4 Å. Thus, in *Tc*AChE, the cross-section at the narrowest point of the bottleneck is ~5 Å [4]. In mouse acetylcholinesterase (mAChE), the narrowest point of the bottleneck has a cross-section of 2.4 Å [5]. Fig. 1 displays the crystal structure of the complex with ACh of the S203A mutant of mAChE. Space-filling representations of two ACh molecules are seen, one lodged above the bottleneck, and one below it [6]. This

Abbreviations: ACh, acetylcholine; AChE, acetylcholinesterase; ATCh, acetylthiocholine; BSF, benzenesulfonyl fluoride; DFP, di*iso*propylphosphorofluoridate; *Ee*AChE, *Electrophorus electricus* AChE; hAChE, human acetylcholinesterase; HupA, (−)-huperzine A; MD, molecular dynamics; MM, molecular mechanics; mAChE, mouse acetylcholinesterase; PMSF, phenylmethylsulfonyl fluoride; RMSD, root-mean-square deviation; RMSF, root-mean-square fluctuation; Russian VX, *O*-isobutyl *S*-[*N*,*N*-diethylaminoethyl]methylphosphonothiolate; *Tc*AChE, *Torpedo californica* acetylcholinesterase; VDW, van der Waals; VX, *O*-ethyl *S*-[*N*,*N*-diisopropylaminoethyl]methylphosphonothiolate; XP, extra precision

* Corresponding author. Department of Structural Biology, Weizmann Institute of Science, Rehovot, 7610001, Israel.
** Corresponding author. Department of Neurobiology, Weizmann Institute of Science, Rehovot, 7610001, Israel.
E-mail addresses: Israel.Silman@weizmann.ac.il (I. Silman), gershom@weizmann.ac.il (J.M.L. Martin), Joel.Sussman@weizmann.ac.il (J.L. Sussman).

https://doi.org/10.1016/j.cbi.2019.06.028
Received 15 March 2019; Received in revised form 4 June 2019; Accepted 13 June 2019
Available online 19 June 2019
0009-2797/

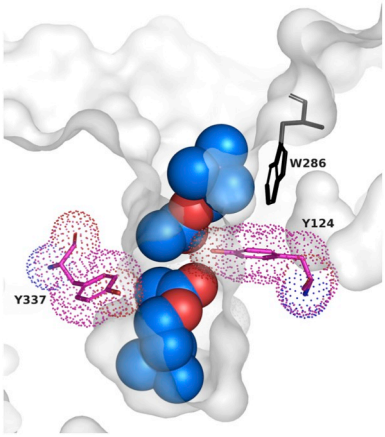

Fig. 1. Space-filling representations of two ACh molecules in the active-site gorge of mAChE. The illustration is based on the PDB ID 2HA4 crystal structure [6]. The two AChs are positioned above and below the bottleneck residues, Y337 and Y124, which are displayed as sticks, with magenta dots displaying their full space-filling surface; the surface of the gorge as a whole is displayed in grey.

representation clearly illustrates that the AChE molecule needs to 'breathe' substantially in order for the ACh molecule to pass through the bottleneck to reach the active site.

AChE is the target of a repertoire of inhibitors that act by covalent modification of its active-site serine. These include organophosphate (OP) nerve agents, and both OP and carbamate insecticides [7]. Phenylmethylsulfonyl fluoride (PMSF) is a sulfonylating agent commonly employed as a non-specific inhibitor of serine proteases [8]. It was reported by Fahrney & Gold [9] that *Electrophorus electricus* AChE (*Ee*AChE) is resistant to inhibition by PMSF, although it was later reported that it is indeed inhibited, but extremely slowly [10,11]. It was subsequently shown that mammalian AChEs are very susceptible to inhibition by PMSF [12].

In an earlier study, we reported that AChE from the electric organ of another electric fish, *Tc*AChE, is also resistant to PMSF, but is irreversibly inhibited very effectively by its homolog, benzenesulfonyl fluoride (BSF) (Scheme 1) [13]. In contrast, we found that mAChE is very well inhibited by both PMSF and BSF. These observations are puzzling because the crystal structures of *Tc*AChE [4] and mAChE [14] are very similar (Fig. 2), as are the kinetic constants for their extremely rapid action on their natural substrate, ACh, and on its homolog, acetylthiocholine [15,16]. We subsequently reported that the anti-Alzheimer drug, rivastigmine (Exelon™), carbamylates human acetylcholinesterase (hAChE) > 1600-fold faster than *Tc*AChE [17].

In the following we present theoretical evidence, using rigid docking in tandem with molecular dynamics (MD) simulations, which shows that differences in flexibility of *Tc*AChE and mammalian AChEs can account for the striking differences experimentally observed in their

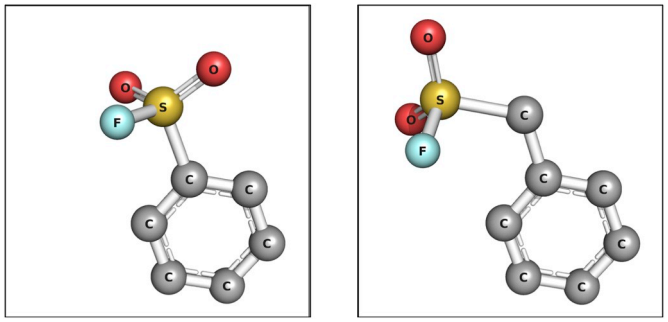

Scheme 1. Stick representations of benzenesulfonyl fluoride (BSF, left) and phenylmethylsulfonyl fluoride (PMSF, right).

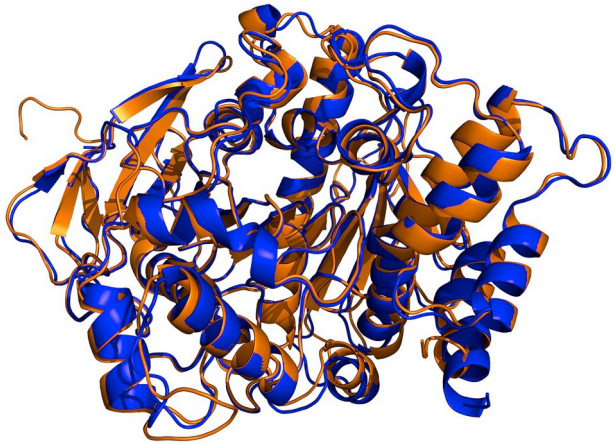

Fig. 2. Overlay of cartoon representations of the crystal structures of *Tc*AChE (blue) and mAChE (orange) looking down the active-site gorge. (For interpretation of the references to colour in this figure legend, the reader is referred to the Web version of this article.)

rates of inhibition by both sulfonylating and carbamylating agents [13,17,18]. Thus, reliance on docking data alone in the context of drug design has the potential to produce very misleading results.

2. Methods

2.1. Docking simulations

The crystal structures of *Tc*AChE (PDB ID: 1EA5 [19,20], 1.8 Å resolution) and mAChE (PDB ID: 5DTI [21], 2.0 Å resolution) were retrieved from the RCSB Protein Data Bank (http://www.rcsb.org). The monomers of Chain A were used for all the simulations [22].

Protein Preparation for Docking and Molecular Dynamics: The 1EA5 and 5DTI structures were prepared with Protein Preparation Wizard [23,24] in Maestro-v11.1 [25], prior to grid-based-ligand docking (GLIDE) [26,27] and MD studies, with the following modifications.

- All waters and cofactors were removed
- Assignment of bond orders
- Addition of hydrogen atoms
- Indicating the 3 intramolecular disulfide bonds
- Adding unseen atoms of side chains in both *Tc*AChE and mAChE
- Addition of residues 259–264 (PGGAGG) which are not seen in any mAChE crystal structure (using the Schrodinger suite PRIME application [28])
- The N and C-termini were capped with acetyl (ACE) and N-methylamino (NMA) groups, respectively
- Assignment of ionization states
- All-atom restrained molecular mechanics (MM) minimizations were performed with a termination criterion of 0.18 Å on the heavy (non-hydrogen) atoms by employing the OPLS3 force field [29].

Ligand preparation: Geometries of the two inhibitors, BSF and PMSF, were optimized using the PBE0 hybrid density functional method [30] combined with the cc-pVTZ Gaussian basis set [31]. Calculations were performed with water as the solvent, using the SCRF continuum solvation model [32]. All calculations utilized the Gaussian 09 suite [33]. The parameters of BSF and PMSF were assigned using the OPLS3 force field [29] with the LigPrep [34] tool available in the Schrödinger suite.

Grid Preparation: Due to the large dimensions of the active-site gorge of AChE, we changed the Glide grid box sizes from the default values [35] shown in Fig. 3a to those shown in Fig. 3b, to ensure that all

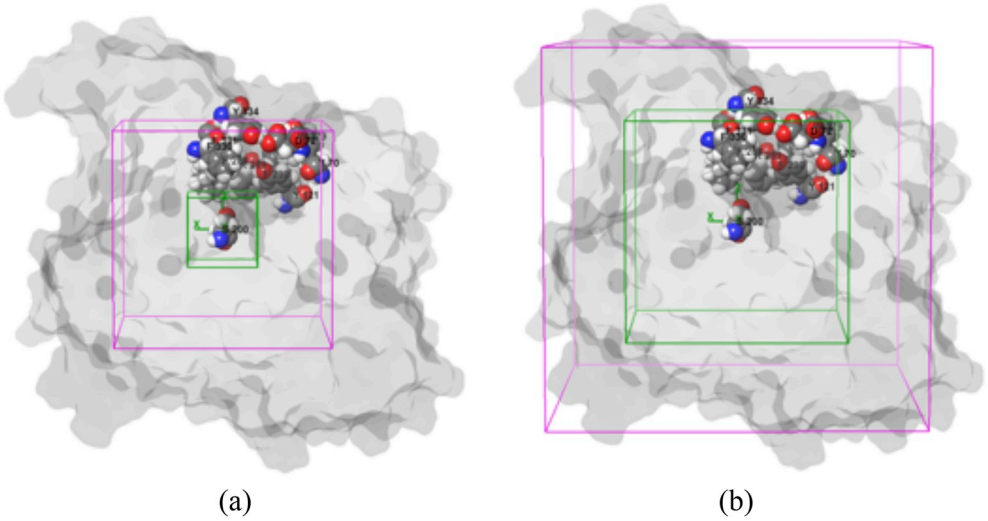

(a) (b)

Fig. 3. Glide grid box settings employed: The boxes were centered around S200(S203),[1] the active-site serine at the bottom of the gorge. (a) Default settings of the inner (green) and outer (magenta) grid boxes were 10x10x10 Å and 30x30 x30 Å, respectively; (b) Inner and outer grid box settings employed for the docking studies on *Tc*AChE and mAChE were 30x30 x30 Å and 50x50 x50 Å, respectively. (For interpretation of the references to colour in the figure legend, the reader is referred to the Web version of the article.)

ligand poses would be located within the purple box. "The outer, purple box defines the volume in which the grid potentials are computed. All ligand atoms of a valid pose must be located within this outer box. The inner, green box defines the volume that the ligand center explores during the exhaustive site-point search" (https://www.schrodinger.com/kb/701).

Glide Docking: Docking, with a rigid protein structure and a flexible ligand, was performed using Schrödinger Glide-v7.4, employing the XP (extra precision) option [27]. One hundred poses were generated per docking calculation. In order to soften the potential for non-polar atoms of the protein (within the grid points) and the ligands, their van der Waals (VDW) radii were scaled to 1.0 Å, with a partial charge cut-off of 0.25 units, while VDW radii of the remaining atoms were not scaled. Glide docking uses a hierarchical clustering algorithm to produce the best set of ligand-binding locations in the defined receptor grid space. The lowest XP glide score for a given ligand indicates the highest binding affinity for the enzyme.

2.2. Molecular dynamics simulations

The Desmond-v4.9 [36] simulation package from Schrödinger was used for MD simulations. The proteins and protein-ligand complex systems were solvated using the explicit SPC [37] solvent model. They were then placed in a cubic box filled with water molecules, such that all protein atoms were at least 10 Å away from the box wall. The MD simulations were performed employing the OPLS3 force field [29]. The charge of the system was neutralized by adding 0.15 M NaCl. The Desmond standard NPT relaxation protocol was used, except that the equilibration time was extended from 24 ps to 5 ns [38]. After the equilibration step, 20 ns and 100 ns MD simulations were performed. The simulations were run on the Faculty of Chemistry HPC (High-Performance Computing) Facility at the Weizmann Institute of Science.

Molecular dynamics (MD) simulations were also carried out with a GPU-accelerated version of the GROMACS 2019 package (https://doi.org/10.5281/zenodo.2424363), using the AMBER ff99SB-ILDN force field [39,40]. The proteins were placed in a cubic box as described above, and solvated by use of the TIP3P water model [41]. NaCl was added to give a concentration of 0.125 M with a small adjustment to achieve a neutrality. Steepest descent energy minimization was applied until the maximum force was $< 1000\ \mathrm{kJ\ mol^{-1}\ nm^{-1}}$. Following the minimization, two simulations with position restraints on the protein were performed independently using an NVT ensemble (100 ps) and an NPT ensemble (5000 ps) employing the modified Berendsen thermostat (velocity-rescaling thermostat (v-rescale)) [42,43] and Parrinello-Rahman barostat [43] coupling algorithms. Finally, five sets of 20 ns MD simulations with different randomized velocities were performed after 5 ns equilibration without position restraints on the protein, using the NPT protocol. Following this, we extended the MD simulations to 100 ns for both mAChE and *Tc*AChE. The simulations were run on the Faculty of Chemistry HPC (High-Performance Computing) Facility at the Weizmann Institute of Science.

3. Results

3.1. Structural comparison of TcAChE and mAChE

The overall structures of the two enzymes closely resemble each other, with root-mean-square deviation (RMSD) values of Cα atoms of 0.54 Å for 449 atoms after protein preparation, and 0.54 Å, for 434 atoms, for the RSCB pdb structures. However, careful inspection reveals three clear differences between the *Tc*AChE and mAChE structures:

(i) There is a difference in one residue at the bottleneck of the active-site gorge, F330 in *Tc*AChE being replaced by Y337 in mAChE, with the sidechains of these two residues being oriented very differently (Fig. 4).
(ii) In mAChE there are four additional residues, P258–P259-G260-G261, which are absent in *Tc*AChE (Fig. 5). This results in a significantly larger loop, with the sequence PPGGAGGN, in mAChE than in *Tc*AChE (Fig. 6).
(iii) In addition to the bottleneck residue, four additional residues in the upper portion of the gorge differ in *Tc*AChE and mAChE: E73(T75), Q74(L76), S81(T83), S124(A127).

3.2. MD simulations of TcAChE and mAChE

Knowledge of the intrinsic flexibility of a protein is important for understanding how structure is linked to function [45]. Accordingly, we performed 20-ns MD simulations on the native crystal structures of *Tc*AChE and mAChE using the Schrödinger MD suite (Fig. 7). Although the 3D structures are almost identical, the MD simulations clearly reveal that mAChE is significantly more flexible than *Tc*AChE. Fig. 7 shows that the average RMSD for the Cα atoms in mAChE is ~1.19 Å, compared to ~0.96 Å in *Tc*AChE. Almost throughout the entire sequence the mAChE residues are more flexible than those of *Tc*AChE (Fig. 8). One of the most flexible regions is around the protruding

[1] Throughout the text, when reference is made to amino acid residues in both *Tc*AChE and mAChE, the *Tc*AChE residue appears first, followed by the corresponding mAChE residue in brackets, *e.g.*, S200(S203).

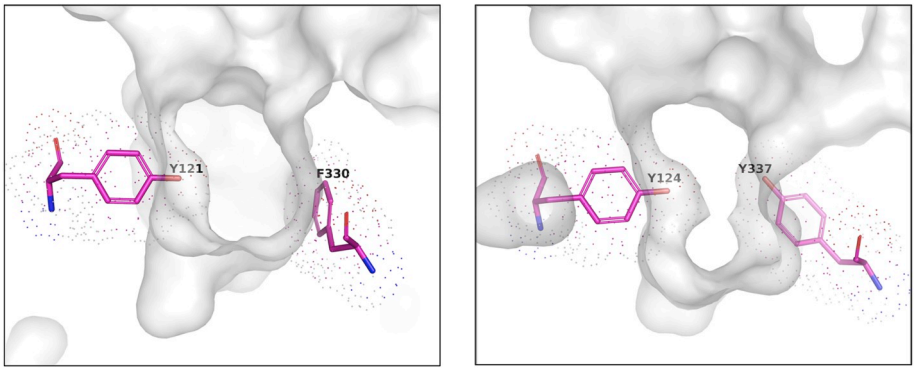

Fig. 4. Comparison of the 3D structures of *Tc*AChE and mAChE in the bottleneck region of the active-site gorge after performance of the protein preparation protocol. The two panels show the orientations of the bottleneck residues Y121(Y124)/F330(Y337) of *Tc*AChE (left) and mAChE (right).

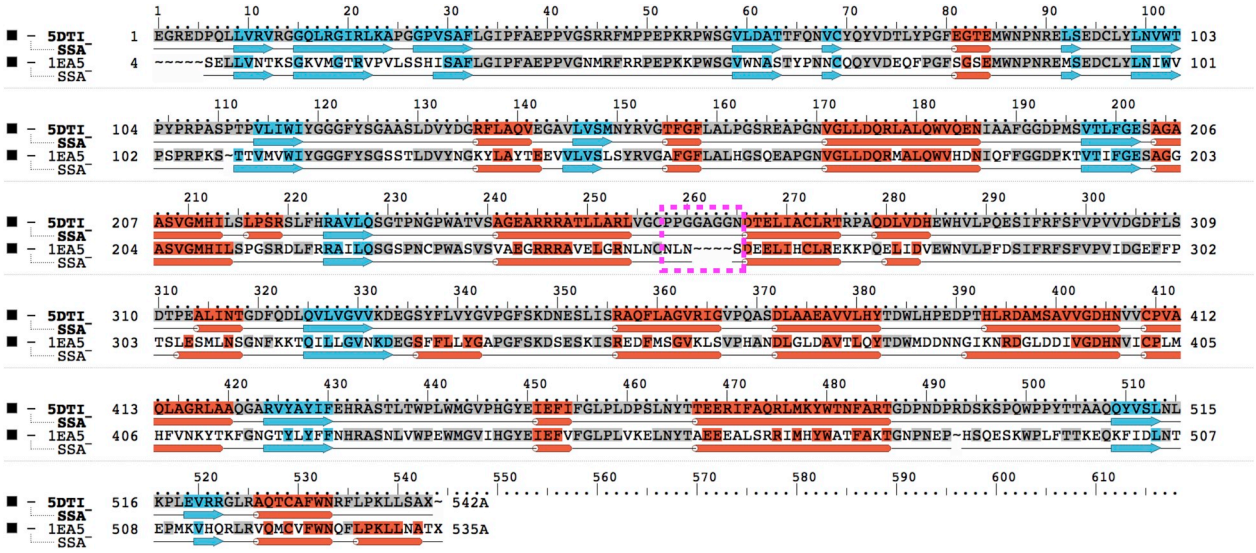

Fig. 5. Pairwise structure-based sequence alignment of *Tc*AChE and mAChE employing the Schrödinger Maestro multiple sequence viewer (MSV) [44]. They possess 58.1% identity and 74.1% similarity. The numbers above the alignment correspond to those of the mAChE sequence. The additional loop in mAChE (PPGGAGGN) is highlighted in magenta. The α-helices, β-strands and loops in the structures of *Tc*AChE and mAChE are represented as cylinders (red), arrows (cyan) and lines (black), respectively. (For interpretation of the references to colour in this figure legend, the reader is referred to the Web version of the article.)

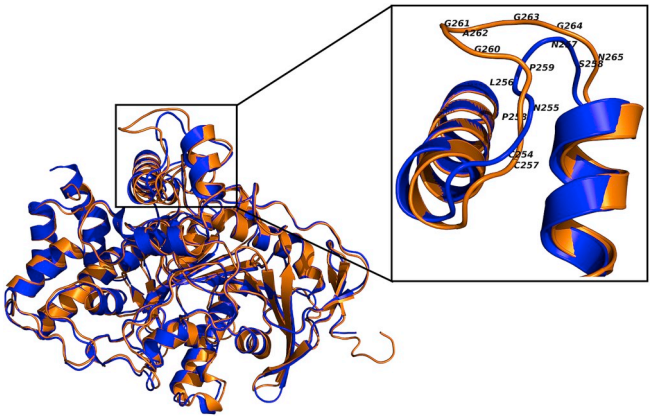

Fig. 6. Superposition of cartoon representations of the crystal structures of *Tc*AChE (blue) and mAChE (orange). The inset (upper right) highlights the large loop present in mAChE. (For interpretation of the references to colour in this figure legend, the reader is referred to the Web version of the article.)

octapeptide sequence in mAChE (Fig. 8). This loop is also present in hAChE, with a very similar sequence, PPGGTGGN [46].

The MD simulations that we obtained are consistent with those previously published for mAChE [47] and for *Tc*AChE [20].

Since these results were so striking, we decided to confirm them by doing MD simulations on *Tc*AChE and mAChE using a different program and force field than that in the Schrödinger package. For this purpose we used a recent GROMACS version together with an Amber Force Field.

We ran five 20 ns-simulations for each for the *Tc*AChE and the mAChE structures. The results fully confirmed those obtained using the Schrödinger package (see Table 1 and Fig. S1 in supporting information). Differences in the RMSD for the Cα-atoms, between the two species, in all these 5 runs, clearly show that *Tc*AChE and mAChE differ in their flexibility. To further verify this, we ran 100 ns simulations for both *Tc*AChE and mAChE. These yielded an average RMSD of 1.297 Å and STD 0.118 Å for *Tc*AChE, and of 1.793 Å and 0.176 Å for mAChE (Fig. 9).

3.3. GlideXP docking of PMSF and BSF into TcAChE and mAChE followed by MD simulation

3.3.1. Docking

No crystal structures are available of complexes or conjugates of BSF or PMSF with AChE. Therefore, we employed a protocol in which docking was followed by MD simulation, as had been done previously for mAChE [48]. GlideXP was used to dock both inhibitors into *Tc*AChE and mAChE. In all four cases, the inhibitors dock at a very similar

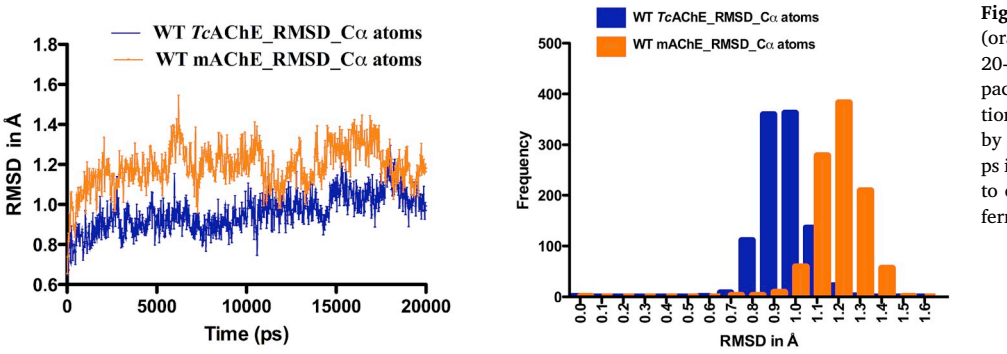

Fig. 7. RMSD values for Cα atoms of mAChE (orange) and *Tc*AChE (blue) obtained from the 20-ns MD simulations using the Desmond package. Left panel, time course of the simulation; right panel, frequency histograms derived by sampling the data displayed on the left at 20-ps intervals. (For interpretation of the references to colour in this figure legend, the reader is referred to the Web version of the article.)

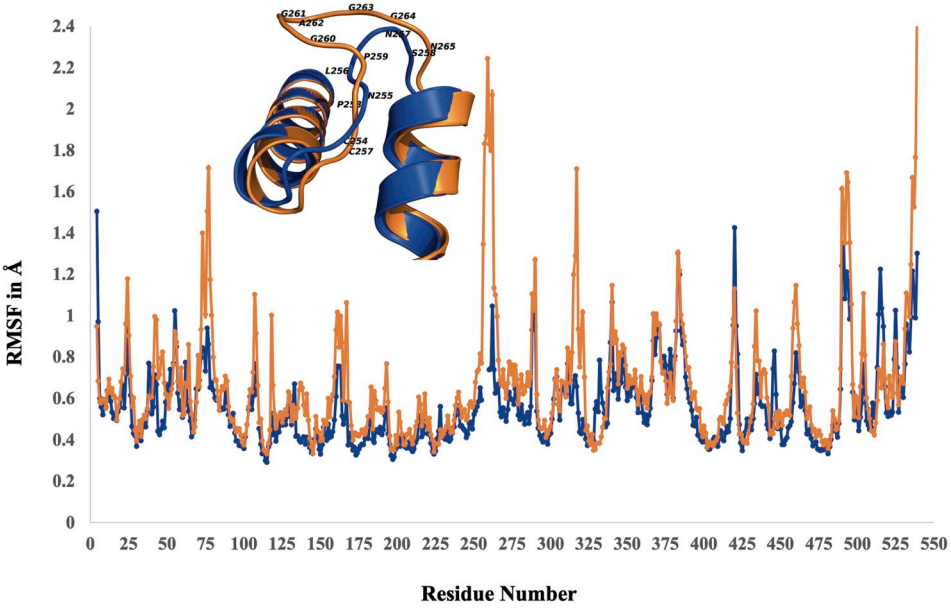

Fig. 8. Root-mean-square fluctuation (RMSF) values for the Cα atoms of mAChE (orange) and *Tc*AChE (blue) obtained from the 20-ns MD simulations. (For interpretation of the references to colour in this figure legend, the reader is referred to the Web version of the article.)

Table 1
20 ns MD simulations for *Tc*AChE and mAChE using GROMACS 2019.

	*Tc*AChE		mAChE	
	RMSD (Å)	STD (Å)	RMSD (Å)	STD (Å)
Run 1	1.158	0.164	1.715	0.277
Run 2	1.281	0.172	1.552	0.122
Run 3	1.219	0.149	1.811	0.229
Run 4	1.080	0.090	1.609	0.205
Run 5	1.150	0.130	1.657	0.230
Averages	**1.178**	**0.141**	**1.669**	**0.213**

position (Fig. 10), with the electrophilic sulfur atom remaining at a great distance from the nucleophilic hydroxyl group of S200(S203) within the active site at the bottom of the gorge (Fig. 10 and Table 2).

3.3.2. MD simulation following docking

Since BSF inhibits both *Tc*AChE and mAChE, whereas PMSF inhibits only mAChE, the docking results displayed in the previous section obviously do not reflect the experimental data. We decided, therefore, to perform MD simulations subsequent to docking [48,49]. It can be clearly seen that after the MD simulation BSF moves close to S200(S203)$O\gamma$ in both *Tc*AChE and mAChE. However, whereas PMSF approaches S203$O\gamma$ in mAChE, it remains distant from S200$O\gamma$ in *Tc*AChE (Fig. 10).

Fig. 11 and Fig. 12 display the MD trajectories for the four cases analyzed, and the histograms derived from them. It can be seen that in the interaction of BSF with *Tc*AChE the ligand approaches S200$O\gamma$ quite closely for part of the time, whereas PMSF remains much further away, above the bottleneck. In the corresponding histograms for interactions with mAChE, the trajectory for BSF almost merges with the magenta line corresponding to the VDW contact distance, while that for PMSF is a little further away. In all four cases, after docking alone the sulfonyl group points up the gorge, away from the active-site, whereas after the MD simulation it points towards the active-site.

4. Discussion

As mentioned in the Introduction, *Tc*AChE, mAChE, and hAChE, act at similar rates on their natural substrate, ACh, and on its homolog, ATCh. They have high sequence homology, and their crystal structures reveal almost identical folds. Yet at least two covalent inhibitors interact several orders of magnitude more rapidly with the mammalian enzymes than with *Tc*AChE [13,17]. It was on this issue that our theoretical study focused. Since *Tc*AChE and the mammalian enzymes do not differ appreciably in their 3D structures [50], steric factors do not seem to explain these very large differences. Consequently, we considered the possibility that differences in their dynamics might provide an explanation. However, it should be kept in mind that, whereas BSF has a planar geometry (Scheme 1), PMSF has a non-planar geometry due to the presence of the additional methylene group, so that its movement through the bottleneck might be expected to be more

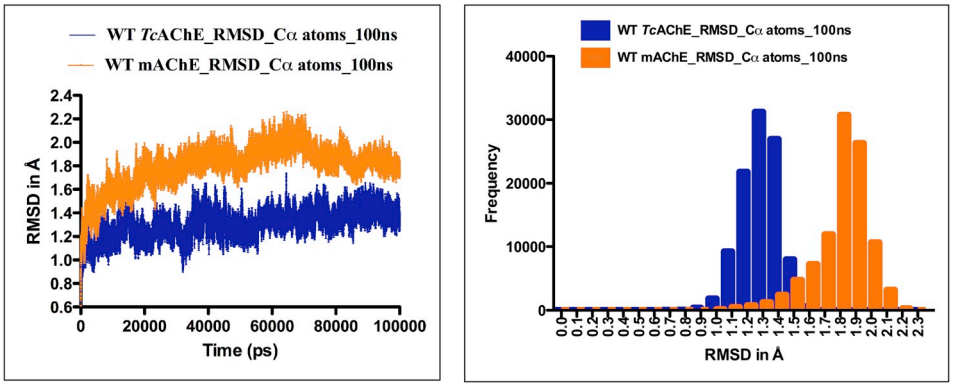

Fig. 9. RMSD values for Cα atoms of mAChE (orange) and *Tc*AChE (blue) obtained from the 100-ns MD simulations that utilized GROMACS 2019. Left panel, time courses of the simulations; right panel, frequency histograms derived by sampling the data displayed on the left at 1-ps intervals. (For interpretation of the references to colour in this figure legend, the reader is referred to the Web version of the article.)

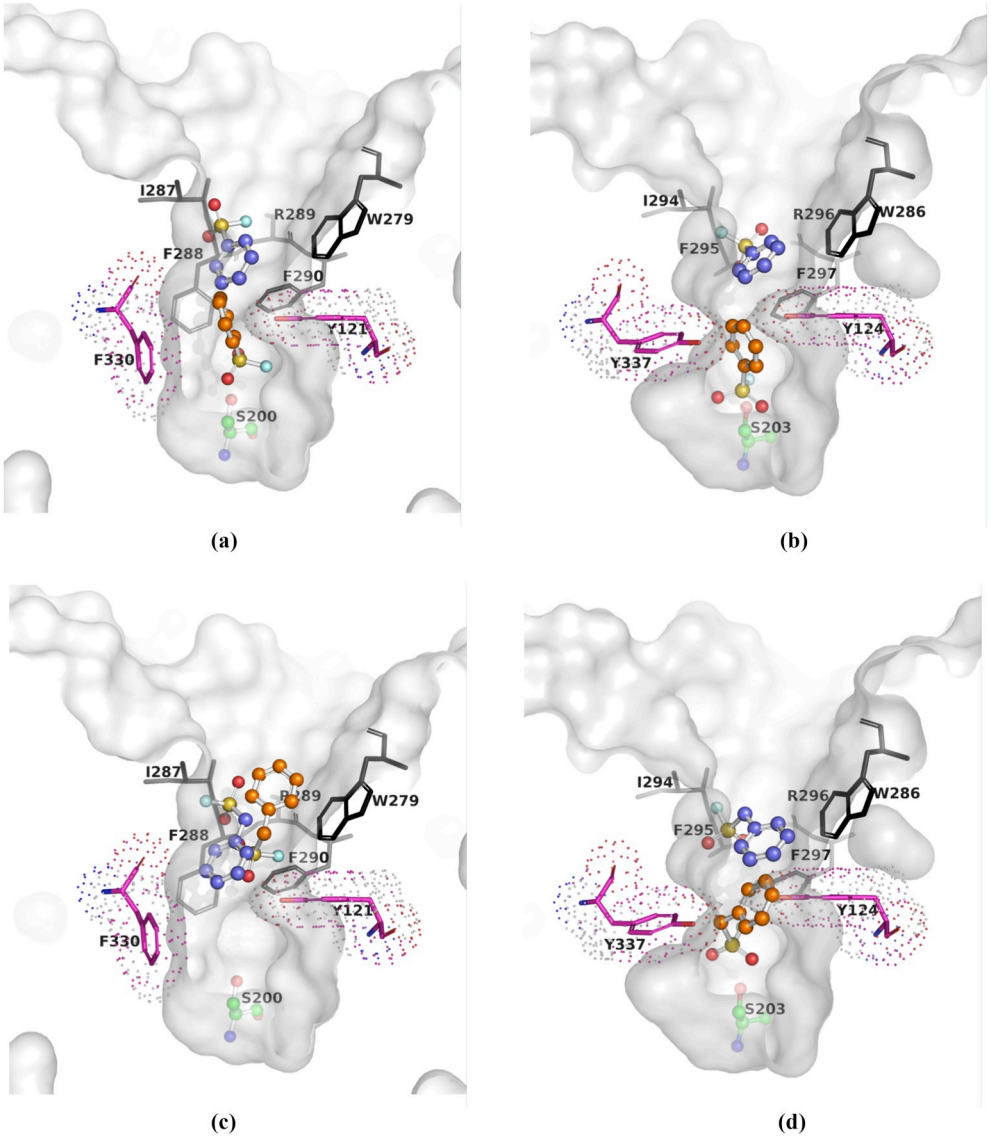

Fig. 10. GlideXP docking and MD simulations for interaction of BSF and PMSF with *Tc*AChE and mAChE. The upper panels show the data obtained for interaction of BSF with (a) *Tc*AChE and (b) mAChE. The lower panels show the data obtained for interaction of PMSF with (c) *Tc*AChE and (d) mAChE. In all four panels two copies of the ligand are displayed. One shows the position of the ligand after docking alone (blue), and the other shows the position after docking followed by MD simulation (orange). It should be noted that the orientations of the amino-acid side-chains displayed are those seen prior to the MD simulations. (For interpretation of the references to colour in this figure legend, the reader is referred to the Web version of the article.)

restricted than that of BSF.

Figs. 7 and 8 clearly show large differences in flexibility between *Tc*AChE and mAChE. mAChE is much more flexible than *Tc*AChE along most of the polypeptide chain, displaying an RMSD for Cα atoms of 1.19 Å *vs* 0.96 Å for *Tc*AChE. The differences in flexibility were verified via 100 ns simulations for both *Tc*AChE and mAChE using GROMACS and an Amber Force Field as shown in Fig. 9. Particularly high flexibility is seen for an octapeptide loop that includes residues P258–P259-G260-G261, which are absent in *Tc*AChE (Figs. 7, Figs. 8 and 9). We thus considered it plausible that the increased flexibility of this loop in mAChE might permit movement of PMSF through the bottleneck in mAChE but not in *Tc*AChE. It is interesting to note that this 4-residue sequence is absent also in *Ee*AChE [51], which, as already noted, is also resistant to PMSF [9]. We already noted that of the two residues at the bottleneck, one is identical in *Tc*AChE and mAChE, *viz.*, Y121(Y124), whereas the other differs, *viz.*, F330(Y337). It is unlikely, however, that

Table 2
Distances between S200(S203)$O\gamma$ of *Tc*AChE and mAChE and the sulfur atom of BSF or PMSF after docking alone or after docking followed by MD simulation.

	*Tc*AChE		mAChE	
	Docked	MD	Docked	MD
BSF	11.8 Å	4.5 Å	10.2 Å	3.0 Å
PMSF	11.8 Å	11.2 Å	10.2 Å	4.0 Å

The MD values displayed refer to the closest approach of the sulfur atom of the ligand to the active-site S200(S203)$O\gamma$ throughout the entire MD trajectory.

suggested that breathing motions might be involved in controlling access of PMSF to the active site. The double mutation, F288L/F290V, which enlarges the acyl pocket, thus permitting *Tc*AChE to act on butyrylthiocholine [52], renders it even more susceptible to PMSF than the WT enzyme [13]. Furthermore, the L282A mutant, which has lower thermal stability than the WT enzyme [53], is inactivated by PMSF at a rate similar to that at which it inactivates the F288L/F290V mutant [13,54]. Thus, in several cases, increased flexibility of AChE appears to be associated with the capacity to be inhibited by PMSF.

As mentioned in the Introduction, the carbamylating agent, rivastigmine, inactivates hAChE (which is highly homologous to mAChE, even more so than *Tc*AChE) three orders of magnitude faster than it inactivates *Tc*AChE [17]. However, various organophosphates (OPs) do not display such differences in rates of phosphorylation of *Tc*AChE and hAChE. Thus, the rates of inactivation of *Tc*AChE and hAChE by di*iso*propylphosphorofluoridate (DFP) are quite similar [55], and the potent *S* isomers of *O*-ethyl *S*-[*N*,*N*-diisopropylaminoethyl]methylphosphonothiolate (VX) and *O*-isobutyl *S*-[*N*,*N*-diethylaminoethyl] methylphosphonothiolate (Russian VX) actually inactivate *Tc*AChE a few-fold faster than hAChE (Y. Ashani, personal communication). Another interesting case for comparison is that of (−)-huperzine A (HupA). This is a bulky alkaloid with a rigid structure and diameter of 9.8 Å. Although HupA is a reversible inhibitor, it inhibits AChE with extremely slow rates of association and disassociation [56]. MD and steered MD simulations show that sizeable distortions of the residues along the active-site gorge are required for it to pass the bottleneck [57–59]. Yet the rates of inhibition of *Tc*AChE and hAChE by HupA are very similar [56]. It is obvious that our understanding of how protein function is coupled to protein dynamics is inadequate, to say the least.

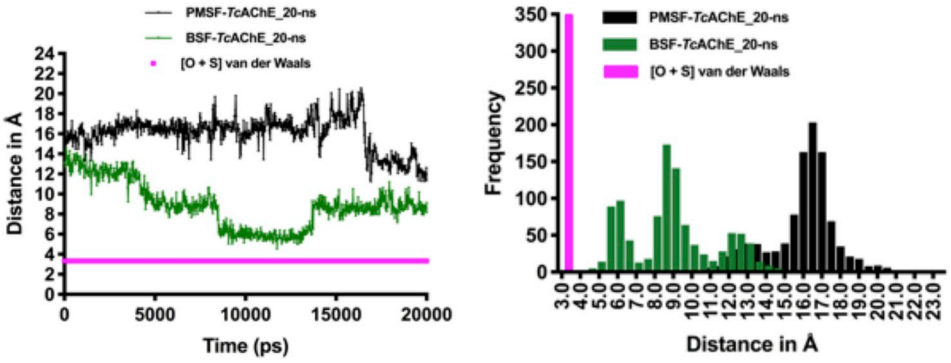

Fig. 11. MD trajectories for interaction of PMSF and BSF with *Tc*AChE. Left, 20-ns trajectories showing BSF-*Tc*AChE (green) and PMSF-*Tc*AChE (black); the magenta line represents the minimum distance between the sulfur atom of the inhibitor and S200$O\gamma$ in a productive encounter. Right, frequency histograms derived by sampling the data displayed on the left at 20-ps intervals. (For interpretation of the references to colour in this figure legend, the reader is referred to the Web version of the article.)

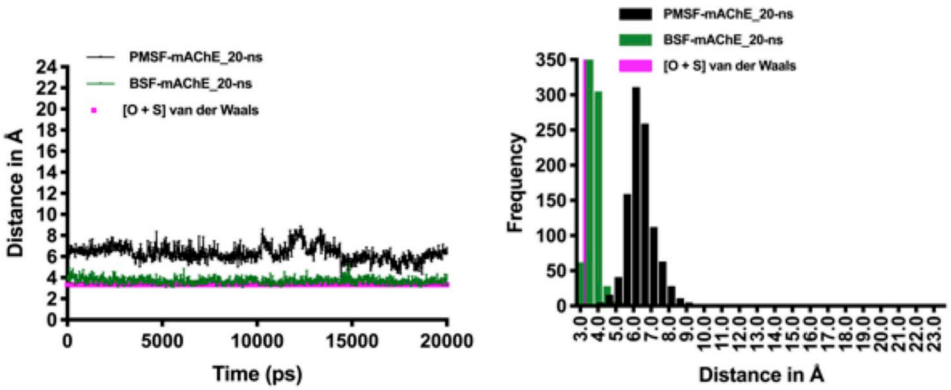

Fig. 12. MD trajectories for interaction of PMSF and BSF with mAChE. Left, 20-ns trajectories showing BSF-mAChE (green) and PMSF-mAChE (black); the magenta line represents the minimum distance between the sulfur atom of the inhibitor and S203$O\gamma$ in a productive encounter. Right, frequency histograms derived by sampling the data displayed on the left at 20-ps intervals. (For interpretation of the references to colour in this figure legend, the reader is referred to the Web version of the article.)

this difference influences the susceptibility to PMSF, since in *Ee*AChE this residue is a tyrosine [51], as in mAChE, rather than a phenylalanine, as in *Tc*AChE.

The results of docking and MD simulations of the WT enzymes by BSF and PMSF mimic the experimental data; thus, BSF comes close to the active-site serine $O\gamma$ atom in both AChEs, but while this is also the case for PMSF binding to mAChE, for *Tc*AChE it remains above the bottleneck, near the top of the gorge, close to the position it occupied in the docking protocol alone.

It should be noted that in all cases, after docking alone both PMSF and BSF were oriented with their sulfonyl moiety pointing up the gorge, away from the active site. But when docking was followed by the MD protocol, in all cases the molecule flipped ~180°, so that the sulfonyl moiety pointed towards the active-site S200(S203)$O\gamma$. This was true also for PMSF interacting with *Tc*AChE, even though in this case the ligand did not cross the bottleneck. In the crystal structure of S203A mAChE referred to in the Introduction (PDB ID 2HA4) [6] two copies of the substrate, ACh, are seen, one below the bottleneck, and one trapped above it. That trapped above it is oriented, like PMSF and BSF after docking followed by MD simulation, with its leaving group facing into the bottleneck, and its quaternary group making a π-cation interaction with W286 in the peripheral anionic site.

Experimental mutagenesis studies that we performed earlier also

JMLM acknowledges funding from the Israel Science Foundation (grant 1358/15), from the Weizmann Institute's SABRA (Supporting Advanced Basic Research) program, the latter supported by a grant

from the Estate of Emile Mimran and the Kimmelman Center for Biomolecular Structure and Assembly. We thank Prof. Koby Levy, Dr. Harry M. Greenblatt, Dr. Efrat Ben-Zeev and Dr. Chakrapani Subramanyam for valuable discussions. We are grateful to the reviewers for their constructive suggestions and comments.

Conflicts of interest

All the authors declare that there are no conflicts of interest related to the publishing of this manuscript on CBI as stated in the signed copies of the Chemico-Biological Interactions Conflict of Interest policy attached to this submission.

Appendix A. Supplementary data

Supplementary data to this article can be found online at https://doi.org/10.1016/j.cbi.2019.06.028.

Transparency document

Transparency document related to this article can be found online at https://doi.org/10.1016/j.cbi.2019.06.028.

References

[1] C. Legay, Why so many forms of acetylcholinesterase? Microsc. Res. Tech. 49 (2000) 56–72.
[2] R.L. Rotundo, Expression and localization of acetylcholinesterase at the neuromuscular junction, J. Neurocytol. 32 (2003) 743–766.
[3] M. Bazelyansky, C. Robey, J.F. Kirsch, Fractional diffusion-limited component of reactions catalyzed by acetylcholinesterase, Biochemistry 25 (1986) 125–130.
[4] J.L. Sussman, M. Harel, F. Frolow, C. Oefner, A. Goldman, L. Toker, I. Silman, Atomic structure of acetylcholinesterase from *Torpedo californica*: a prototypic acetylcholine-binding protein, Science 253 (1991) 872–879.
[5] T. Shen, K. Tai, R.H. Henchman, J.A. McCammon, Molecular dynamics of acetylcholinesterase, Acc. Chem. Res. 35 (2002) 332–340.
[6] Y. Bourne, Z. Radic, G. Sulzenbacher, E. Kim, P. Taylor, P. Marchot, Substrate and product trafficking through the active center gorge of acetylcholinesterase analyzed by crystallography and equilibrium binding, J. Biol. Chem. 281 (2006) 29256–29267.
[7] C.B. Millard, C.A. Broomfield, Anticholinesterases: medical applications of neurochemical principles, J. Neurochem. 64 (1995) 1909–1918.
[8] T. Le, H.J. Lee, H.J. Jin, An efficient method to eliminate the protease activity contaminating commercial bovine pancreatic DNase I, Anal. Biochem. 483 (2015) 4–6.
[9] D.E. Fahrney, A.M. Gold, Sulfonyl fluorides as inhibitors of esterases. I. Rates of reaction with acetylcholinesterase, alpha-chymotrypsin and trypsin, J. Am. Chem. Soc. 85 (1963) 997–1000.
[10] P. Barnett, T.L. Rosenberry, Inactivation of *Electrophorus electricus* acetylcholinesterase by benzenemethane sulfonylfluoride, Arch. Biochem. Biophys. 190 (1978) 202–205.
[11] D.E. Moss, D.E. Fahrney, Kinetic analysis of differences in brain acetylcholinesterase from fish or mammalian sources, Biochem. Pharmacol. 27 (1978) 2693–2698.
[12] P. Turini, S. Kurooka, M. Steer, A.N. Corbascio, T.P. Singer, The action of phenylmethylsulfonyl fluoride on human acetylcholinesterase, chymotrypsin and trypsin, J. Pharmacol. Exp. Ther. 167 (1969) 98–104.
[13] D. Kraut, H. Goff, R.K. Pai, N.A. Hosea, I. Silman, J.L. Sussman, P. Taylor, J.G. Voet, Inactivation studies of acetylcholinesterase with phenylmethanesulfonyl fluoride, Mol. Pharmacol. 57 (2000) 1243–1248.
[14] Y. Bourne, P. Taylor, P.E. Bougis, P. Marchot, Crystal structure of mouse acetylcholinesterase. A peripheral site-occluding loop in a tetrameric assembly, J. Biol. Chem. 274 (1999) 2963–2970.
[15] M. Vigny, S. Bon, J. Massoulié, F. Leterrier, Active-site catalytic efficiency of acetylcholinesterase molecular forms in *Electrophorus, Torpedo*, rat and chicken, Eur. J. Biochem. 85 (1978) 317–323.
[16] D.C. Vellom, Z. Radic, Y. Li, N.A. Pickering, S. Camp, P. Taylor, Amino acid residues controlling acetylcholinesterase and butyrylcholinesterase specificity, Biochemistry 32 (1993) 12–17.
[17] P. Bar-On, C.B. Millard, M. Harel, H. Dvir, A. Enz, J.L. Sussman, I. Silman, Kinetic and structural studies on the interaction of cholinesterases with the anti-Alzheimer drug rivastigmine, Biochemistry 41 (2002) 3555–3564.
[18] M.R. Ali, M. Sadoqi, S.G. Moller, A. Boutajangout, M. Mezei, Assessing the binding of cholinesterase inhibitors by docking and molecular dynamics studies, J. Mol. Graph. Model. 76 (2017) 36–42.
[19] H. Dvir, H.L. Jiang, D.M. Wong, M. Harel, M. Chetrit, X.C. He, X.C. Tang, I. Silman, D.L. Bai, J.L. Sussman, X-ray structures of *Torpedo californica* acetylcholinesterase complexed with (+)-Huperzine A and (-)-Huperzine B: structural evidence for an active site rearrangement, Biochemistry 41 (2002) 10810–10818.
[20] Y. Xu, J.-P. Colletier, M. Weik, H. Jiang, J. Moult, I. Silman, J.L. Sussman, Flexibility of aromatic residues in the active-site gorge of acetylcholinesterase: X-ray versus molecular dynamics, Biophys. J. 95 (2008) 2500–2511.
[21] F.S. Katz, S. Pecic, T.H. Tran, I. Trakht, L. Schneider, Z. Zhu, L. Ton-That, M. Luzac, V. Zlatanic, S. Damera, J. Macdonald, D.W. Landry, L. Tong, M.N. Stojanovic, Discovery of new classes of compounds that reactivate acetylcholinesterase inhibited by organophosphates, Chembiochem 16 (2015) 2205–2215.
[22] S. Cheng, W. Song, X. Yuan, Y. Xu, Gorge motions of acetylcholinesterase revealed by microsecond molecular dynamics simulations, Sci. Rep. 7 (2017) 3219.
[23] G.M. Sastry, M. Adzhigirey, T. Day, R. Annabhimoju, W. Sherman, Protein and ligand preparation: parameters, protocols, and influence on virtual screening enrichments, J. Comput. Aided Mol. Des. 27 (2013) 221–234.
[24] Protein Preparation Wizard - Schrödinger Release 2017-1, Schrödinger, LLC, New York, NY, 2017.
[25] Maestro - Schrödinger Release 2017-1, Schrödinger, LLC, New York, NY, 2017.
[26] R.A. Friesner, J.L. Banks, R.B. Murphy, T.A. Halgren, J.J. Klicic, D.T. Mainz, M.P. Repasky, E.H. Knoll, M. Shelley, J.K. Perry, D.E. Shaw, P. Francis, P.S. Shenkin, Glide: A new approach for rapid, accurate docking and scoring. 1. Method and assessment of docking accuracy, J. Med. Chem. 47 (2004) 1739–1749.
[27] R.A. Friesner, R.B. Murphy, M.P. Repasky, L.L. Frye, J.R. Greenwood, T.A. Halgren, P.C. Sanschagrin, D.T. Mainz, Extra precision glide: docking and scoring incorporating a model of hydrophobic enclosure for protein-ligand complexes, J. Med. Chem. 49 (2006) 6177–6196.
[28] PRIME, Schrödinger, Release 2017-1, Schrödinger, LLC, New York, NY, 2017.
[29] E. Harder, W. Damm, J. Maple, C. Wu, M. Reboul, J.Y. Xiang, L. Wang, D. Lupyan, M.K. Dahlgren, J.L. Knight, J.W. Kaus, D.S. Cerutti, G. Krilov, W.L. Jorgensen, R. Abel, R.A. Friesner, OPLS3: a force field providing broad coverage of drug-like small molecules and proteins, J. Chem. Theory Comput. 12 (2016) 281–296.
[30] J.P. Perdew, K. Burke, M. Ernzerhof, Generalized gradient approximation made simple, Phys. Rev. Lett. 77 (1996) 3865–3868.
[31] T.H. Dunning, Gaussian basis sets for use in correlated molecular calculations. I. The atoms boron through neon and hydrogen, J. Chem. Phys. 90 (1989) 1007–1023.
[32] M. Cossi, G. Scalmani, N. Rega, V. Barone, New developments in the polarizable continuum model for quantum mechanical and classical calculations on molecules in solution, J. Chem. Phys. 117 (2002) 43–54.
[33] M.J. Frisch, G.W. Trucks, H.B. Schlegel, G.E. Scuseria, M.A. Robb, J.R. Cheeseman, G. Scalmani, V. Barone, G.A. Petersson, H. Nakatsuji, X. Li, M. Caricato, A. Marenich, J. Bloino, B.G. Janesko, R. Gomperts, B. Mennucci, H.P. Hratchian, J.V. Ortiz, A.F. Izmaylov, J.L. Sonnenberg, D. Williams-Young, F. Ding, F. Lipparini, F. Egidi, J. Goings, B. Peng, A. Petrone, T. Henderson, D. Ranasinghe, V.G. Zakrzewski, J. Gao, N. Rega, G. Zheng, W. Liang, M. Hada, M. Ehara, K. Toyota, R. Fukuda, J. Hasegawa, M. Ishida, T. Nakajima, Y. Honda, O. Kitao, H. Nakai, T. Vreven, K. Throssell, J. Montgomery, J. A, J.E. Peralta, F. Ogliaro, M. Bearpark, J.J. Heyd, E. Brothers, K.N. Kudin, V.N. Staroverov, T. Keith, R. Kobayashi, J. Normand, K. Raghavachari, A. Rendell, J.C. Burant, S.S. Iyengar, J. Tomasi, M. Cossi, J.M. Millam, M. Klene, C. Adamo, R. Cammi, J.W. Ochterski, R.L. Martin, K. Morokuma, O. Farkas, J.B. Foresman, F.D. J, Gaussian 09, Revision A.02, Gaussian, Inc., Wallingford, CT, 2009.
[34] LigPrep - Schrödinger Release 2017-1, Schrödinger, LLC, New York, NY, 2017.
[35] L. Berg, C.D. Andersson, E. Artursson, A. Hornberg, A.K. Tunemalm, A. Linusson, F. Ekstrom, Targeting acetylcholinesterase: identification of chemical leads by high throughput screening, structure determination and molecular modeling, PLoS One 6 (2011) e26039.
[36] Desmond Molecular Dynamics System - Schrödinger Release 2017-1, Schrödinger, LLC, New York, NY, 2017.
[37] Y. Wu, H.L. Tepper, G.A. Voth, Flexible simple point-charge water model with improved liquid-state properties, J. Chem. Phys. 124 (2006) 024503.
[38] Z. Guo, U. Mohanty, J. Noehre, T.K. Sawyer, W. Sherman, G. Krilov, Probing the alpha-helical structural stability of stapled p53 peptides: molecular dynamics simulations and analysis, Chem. Biol. Drug Des. 75 (2010) 348–359.
[39] V. Hornak, R. Abel, A. Okur, B. Strockbine, A. Roitberg, C. Simmerling, Comparison of multiple Amber force fields and development of improved protein backbone parameters, Proteins 65 (2006) 712–725.
[40] K. Lindorff-Larsen, S. Piana, K. Palmo, P. Maragakis, J.L. Klepeis, R.O. Dror, D.E. Shaw, Improved side-chain torsion potentials for the Amber ff99SB protein force field, Proteins 78 (2010) 1950–1958.
[41] W.L. Jorgensen, J. Chandrasekhar, J.D. Madura, R.W. Impey, M.L. Klein, Comparison of simple potential functions for simulating liquid water, J. Chem. Phys. 79 (1983) 926–935.
[42] G. Bussi, D. Donadio, M. Parrinello, Canonical sampling through velocity rescaling, J. Chem. Phys. 126 (2007) 014101-014107.
[43] M. Parrinello, A. Rahman, Polymorphic transitions in single crystals: a new molecular dynamics method, J. Appl. Phys. 52 (1981) 7182–7190.
[44] J. Jusuf, S. Krystek, Multiple Sequence Viewer, Schrödinger, LLC, New York, N.Y., 2017.
[45] P. Eastman, M. Pellegrini, S. Doniach, Protein flexibility in solution and in crystals, J. Chem. Phys. 110 (1999) 10141–10152.
[46] H. Soreq, R. Ben-Aziz, C.A. Prody, S. Seidman, A. Gnatt, L. Neville, J. Lieman-Hurwitz, E. Lev-Lehman, D. Ginzberg, Y. Lapidot-Lifson, H. Zakut, Molecular cloning and construction of the coding region for human acetylcholinesterase reveals a G + C-rich attenuating structure, Proc. Natl. Acad. Sci. U.S.A. 87 (1990) 9688–9692.
[47] S. Tara, T.P. Straatsma, J.A. McCammon, Mouse acetylcholinesterase unliganded and in complex with Huperzine A: a comparison of molecular dynamics simulations, Biopolymers 50 (1999) 35–43.

[48] S. Tara, V. Helms, T.P. Straatsma, J.A. McCammon, Molecular dynamics of mouse acetylcholinesterase complexed with huperzine A, Biopolymers 50 (1999) 347–359.
[49] H. Alonso, A.A. Bliznyuk, J.E. Gready, Combining docking and molecular dynamic simulations in drug design, Med. Res. Rev. 26 (2006) 531–568.
[50] G. Kryger, M. Harel, K. Giles, L. Toker, B. Velan, A. Lazar, C. Kronman, D. Barak, N. Ariel, A. Shafferman, I. Silman, J.L. Sussman, Structures of recombinant native and E202Q mutant human acetylcholinesterase complexed with the snake-venom toxin fasciculin-II, Acta Crystallogr. D Biol. Crystallogr. 56 (2000) 1385–1394.
[51] S. Simon, J. Massoulié, Cloning and expression of acetylcholinesterase from *Electrophorus*. Splicing pattern of the 3' exons in vivo and in transfected mammalian cells, J. Biol. Chem. 272 (1997) 33045–33055.
[52] M. Harel, J.L. Sussman, E. Krejci, S. Bon, P. Chanal, J. Massoulié, I. Silman, Conversion of acetylcholinesterase to butyrylcholinesterase: modeling and mutagenesis, Proc. Natl. Acad. Sci. U.S.A. 89 (1992) 10827–10831.
[53] N. Morel, S. Bon, H.M. Greenblatt, D. Van Belle, S.J. Wodak, J.L. Sussman, J. Massoulié, I. Silman, Effect of mutations within the peripheral anionic site on the stability of acetylcholinesterase, Mol. Pharmacol. 55 (1999) 982–992.
[54] D. Kraut, N. Morel, S. Bon, J. Massoulié, I. Silman, J.L. Sussman, J.G. Voet, *Torpedo* AChE L282A mutant (destabilized) becomes PMSF sensitive, Biochemistry 39 (2000) 1547.
[55] C.B. Millard, G. Kryger, A. Ordentlich, H.M. Greenblatt, M. Harel, M.L. Raves, Y. Segall, D. Barak, A. Shafferman, I. Silman, J.L. Sussman, Crystal structures of aged phosphonylated acetylcholinesterase: nerve agent reaction products at the atomic level, Biochemistry 38 (1999) 7032–7039.
[56] Y. Ashani, J. Grunwald, C. Kronman, B. Velan, A. Shafferman, Role of tyrosine 337 in the binding of huperzine A to the active site of human acetylcholinesterase, Mol. Pharmacol. 45 (1994) 555–560.
[57] Y. Xu, J. Shen, X. Luo, I. Silman, J.L. Sussman, K. Chen, H. Jiang, How does Huperzine A enter and leave the binding gorge of acetylcholinesterase? Steered molecular dynamics simulations, J. Am. Chem. Soc. 125 (2003) 11340–11349.
[58] F. Bai, Y. Xu, J. Chen, Q. Liu, J. Gu, X. Wang, J. Ma, H. Li, J.N. Onuchic, H. Jiang, Free energy landscape for the binding process of Huperzine A to acetylcholinesterase, Proc. Natl. Acad. Sci. U.S.A. 110 (2013) 4273–4278.
[59] J. Rydzewski, R. Jakubowski, W. Nowak, H. Grubmüller, Kinetics of Huperzine A dissociation from acetylcholinesterase via multiple unbinding pathways, J. Chem. Theory Comput. 14 (2018) 2843–2851.